Photon-emission studies of slow C^{4+}-Ne collisions

M.O. Larsson,* A. Wännström, M. Wang, A. Arnesen, F. Heijkenskjöld, and A. Langereis
Department of Physics, Uppsala University, Box 530, S-751 21 Uppsala, Sweden

B. Nyström
Department of Physics, University of Lund, Sölveg. 14, S-223 62 Lund, Sweden

R.W. McCullough
Department of Pure and Applied Physics, The Queen's University of Belfast, Belfast, United Kingdom

H. Cederquist
Atomic Physics, Stockholm University, Frescativ. 24, S-104 05 Stockholm, Sweden
(Received 8 July 1996)

We present absolute term- and level-selective cross sections for specific single- and double-electron capture processes in slow (16 keV) C^{4+}-Ne collisions. The results are deduced through a combined analysis of earlier translational energy-gain data and the present photon-emission cross sections in the region 40–240 nm. We find that double-electron capture is dominated by processes in which two electrons appear to change orbitals in a single interaction of two diabatic quasimolecular potential curves—a type of process which rarely has been isolated before. Furthermore, we observe a strong preference for population of $2s2p$ over $2p^2$ configurations in these one-step two-electron capture reactions. This is a remarkable configuration selectivity, since reaction channels leading to $2s2p$ and $2p^2$ configurations cross with the incident channel at almost the same internuclear distances. [S1050-2947(97)05001-4]

PACS number(s): 34.70.+e, 34.50. Fa, 36.40.−c

I. INTRODUCTION

The mechanisms behind one- and two-electron capture from neutral atoms to slow ($v<1$ a.u.) multiply charged ions have been studied and discussed extensively during the past decade (for a review see, e.g., Barat and Roncin [1]). There is a vast number of cases where there is overwhelming evidence that single-electron capture (SC) is mostly due to radial coupling between diabatic quasimolecular potential curves. This is true for projectiles of moderate and high charge states. The situation is a little less clear for double-electron capture (DC) where different mechanisms compete. However, it has become possible to express some general rules to which a large part of the research community would agree. For high projectile charge states, where the densities of projectile capture states are high, it appears that the two-step mechanism often dominates. This means that the two electrons are transferred to the projectile sequentially and at different internuclear separations. For moderate projectile charge states, where the densities of available capture states usually are lower, the one-step two-electron transfer mechanism may become dominant. The most well-known example of the latter is two-electron capture in slow C^{4+}-He collisions [2,3].

One way to distinguish between the one- and two-step mechanisms has been to measure the angular distributions for scattered projectiles, preferably with information about the translational energy gain and thus the inelasticity (Q value) of the collision. In most cases, the two-step process can be expected to give considerably larger scattering angles than the one-step process. The latter is sometimes associated with electron correlation. This terminology can be used in the sense that two electrons change orbitals in a single interaction between two diabatic quasimolecular potential curves as in the C^{4+}-He [2,3] and the O^{6+} He cases [4–6]. However, two-step processes can also be discussed in a similar fashion when transfer of the second electron affects the state of the first transferred electron, as in Ar^{16+}-He collisions [7].

Here we have studied single- and double-electron capture in slow C^{4+}-Ne collisions (16 keV) by means of high-resolution photon-emission spectroscopy. The results were analyzed together with recent energy-gain data (for SC and DC) from McCullough *et al.* [8] at the same collision energy. Using this procedure it becomes possible to discriminate between collision processes with close-lying Q values, which were unresolved in earlier studies relying solely on the translational energy-gain technique. This separation reveals, e.g., that double-electron capture is dominated by *one-step* processes and, further, that these processes are much more likely to populate $2s2p$ than $2p^2$ configurations in C^{2+}. Such a configuration selectivity for one-step DC has not been observed before and here it is especially interesting since the amounts of configuration interaction and singlet-triplet mixing are extremely low in the LS terms formed in the $2s2p$ and $2p^2$ populations.

Earlier translational energy-gain measurements on this system have revealed several truly remarkable features. Cederquist *et al.* [3] reported an apparent hole in the reaction window for DC at energies of 400–500 eV ($v\sim0.04$ a.u.); strong population of four (incompletely resolved) channels

*Present address: Aarhus University, Det Fysiske Institut, Nymunkegade 2, DK-8000 Aarhus, Denmark.

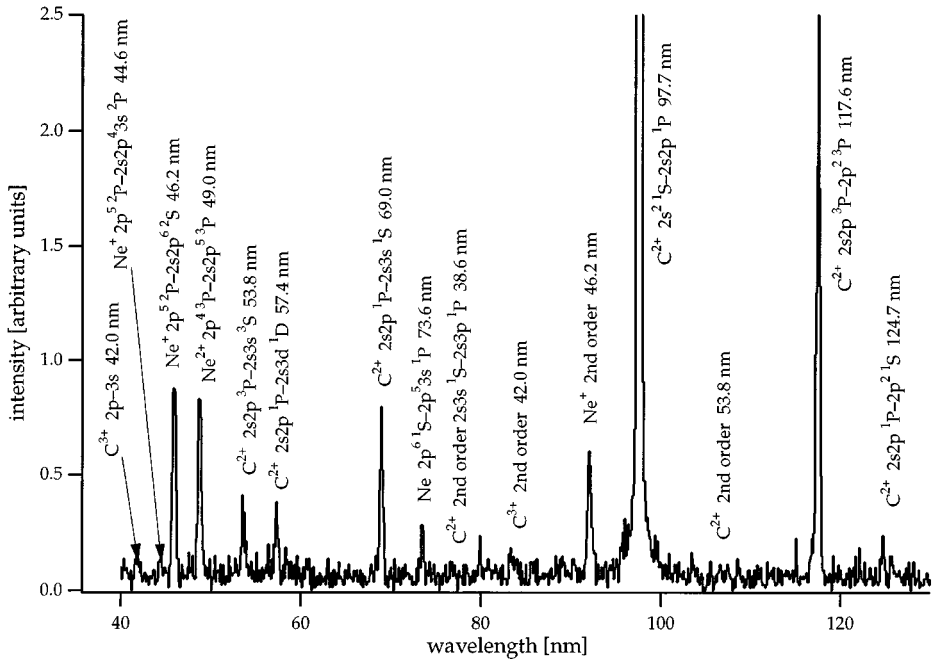

FIG. 1. Photon-emission spectrum for the wavelength region 40–130 nm in 16 keV C^{4+}-Ne collisions (spectrum I). The line intensities are shown in arbitrary units and they are not corrected for the varying spectral sensitivity (cf. text). The intensity for the transition at 97.7 nm is ~80 in the scale used here.

around $Q=30$ eV followed by very weakly populated channels around $Q=20$ eV, and then again strong population of a single channel at $Q=16$ eV. It was speculated that the population of this latter DC channel was somehow related to the dominant SC channel at virtually the same Q value (16 eV) [3]. Keller *et al.* [9] performed measurements of angular distributions in a similar collision energy regime (600–1000 eV) and reported clear evidence for one-step population for the (then unresolved) DC channels around $Q=30$ eV. Further, they found that the intensity in the DC channel at $Q=16$ eV decreased drastically when the energy was increased from 600 to 1000 eV [9].

The experimental technique is described in the next section, while the method to establish a relation between spectral-line intensities and absolute emission cross sections (σ_{em}) is given in Sec. III A. The latter quantities are defined as the absolute cross sections for emission of a single photon (due to a specific atomic transition) during or after the collision. The absolute cross sections for *direct* population of specified atomic terms and levels, i.e., excluding contributions from cascades, are given in Sec. III B. In Sec. IV, we combine these latter results with the energy-gain data (SC and DC) of McCullough *et al.* at 16 keV ($v\sim0.2$ a.u.) [8] and deduce absolute cross sections for collision processes with resolved final quantum states for both the projectile and the target.

II. EXPERIMENT

The experimental setup has previously been described in detail in Refs. [10–12]. Thus we only give a short description here. Carbon ions were produced in a 6.4 GHz electron cyclotron resonance (ECR) ion source and extracted at a potential of 4 kV. The C^{4+} beam was selected by means of a double-focusing 90° dipole magnet and directed through a 7 cm long differentially pumped target cell containing Ne. The ion current, typically 4 μA, was measured with a Faraday cup situated downstream from the cell. The collision-induced photon emission was observed through an 8 mm diameter aperture in the target cell by an evacuated 1 m normal incidence spectrometer.

The radiation emitted perpendicular to the beam direction was recorded in the 40–240 nm wavelength range with two different combinations of detector and grating. Spectrum I (40–130 nm; see Fig. 1) was recorded with a channeltron detector and a 1200 mm^{-1} grating blazed for 75 nm, whereas a photomultiplier tube and a 1200 mm^{-1} grating blazed for 150 nm were used for spectrum II (110–240 nm, see Fig. 2). The spectrometer slit widths were set to 500 μm and 1000 μm, yielding the expected line widths (full width at half maximum) of 0.4 nm and 0.8 nm for spectra I and II, respectively. The number of registered photons per channel was normalized to the accumulated charge in the Faraday cup.

One fine-structure multiplet ($Ne^+\ 2p^5\ ^2P-2s2p^6\ ^2S$ at ~46 nm) in spectrum I was resolved in a separate scan using a slit width of 125 μm. The intensity relation between the lines in this multiplet agreed with tabulated data for Ne^+, ruling out the possibility of a significant contribution to the line intensity from the $2s2p\ ^3P-2s3d\ ^3D$ transitions in C^{2+} (also at ~46 nm).

The Ne pressure in the target gas cell was determined from aperture conductances, the measured pressure in the vacuum volume outside the cell and the pumping speed for Ne in the same volume. This procedure leads to a rather large absolute uncertainty, but since the absolute cross sections determined in the present study are obtained through a normalization procedure this is of little importance. We are, however, confident that the estimated cell pressures are reliable on a relative scale in the pressure range used here (30–120 mPa). Spectra I and II (shown in Figs. 1 and 2) were recorded at a nominal cell pressure of 30 mPa. With a cell length of 7 cm and a total cross section for electron capture of $\sim2\times10^{-15}$ cm^2 (see below), there is a total reaction probability of 10% for each C^{4+} ion which enters the cell at 30 mPa. The intensities of all the individual spectral lines

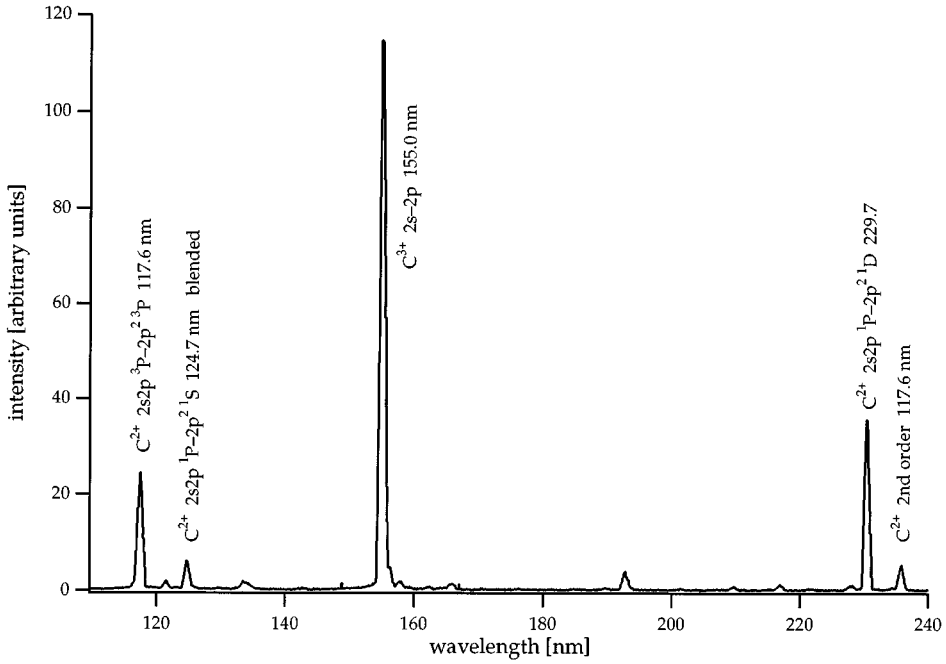

FIG. 2. Photon-emission spectrum for the wavelength region 110–240 nm in 40 keV C^{4+}-Ne collisions (spectrum II). The line intensities are shown in arbitrary units and they are not corrected for the varying spectral sensitivity (cf. text). The important parts of this spectrum were recorded also at the collision energy 16 keV. The absolute cross sections are determined from these latter scans.

discussed in this work were found to increase linearly with the cell pressure. Furthermore, we found no significant influence of anisotropy and polarization effects on the relative line intensities (cf. Hoeckstra *et al.* [13]) when we recorded (parts of) spectrum I with 45° angle with respect to the ion beam.

We calibrated the *relative* detection efficiency in the 40–100 nm wavelength region (spectrum I) by measuring line intensities for 105 keV Xe^{7+}-He and 120 keV Xe^{8+}-He and comparing those to the emission cross sections published by Druetta and Hitz [14]. Spectrum II was intensity calibrated on a relative scale by means of line intensities in photon emission spectra of $10q$ keV Xe^{q+}-T (q=5–8; T=He,Ar) and related atomic branching ratios (Larsson *et al.* [10,12]), calculated with the HFR code (Hartree-Fock with relativistic corrections) from Cowan [15].

III. DETERMINATION OF ABSOLUTE CROSS SECTIONS

A. Calibration of the emission cross-section scale

A *common* and *absolute* emission cross-section scale (σ_{em}) for spectra I and II was obtained by means of three different experimental results at the collision energy of 16 keV: The absolute and total single-electron capture cross section σ_{SC}^{tot} measured by Zwally and Koopmann [16]; the translational energy-gain spectrum for SC measured by McCullough *et al.* [8]; and the present relative intensities of emission lines due to SC in spectra I and II.

According to Zwally and Koopmann [16] $\sigma_{SC}^{tot}=(4.8\pm0.5)\times10^{-16}$ cm^2 at 16 keV. We partitioned σ_{SC}^{tot} on six Gaussian peaks which we fitted to the SC energy-gain spectrum shown in Fig. 3 [8]. The photon-emission spectrum II was then put on an absolute cross-section scale by relating the intensity for $C^{3+}(2s-2p)$ emission at 155.0 nm to the summed absolute cross section ($0.53\times10^{-16}+0.36\times10^{-16}+0.33\times10^{-16}$ cm^2) for the energy-gain peaks C_{SC}, D_{SC}, and E_{SC} (Fig. 3 and Table I). These peaks correspond to collision processes that give rise to $C^{3+}(2s-2p)$ emission, either through direct population of the $C^{3+}(2p)$ configuration (C_{SC} and D_{SC}) or indirectly via cascading from $C^{3+}(3s)$ (E_{SC}; see Fig. 4). Similarly, the absolute emission cross sections for spectrum I are obtained from the intensities of the $2p^5\ ^2P$–$2s2p^6\ ^2S$ (46.1 nm) and $2p^5\ ^2P$ –$2p^4 3s\ ^2P$ (44.6 nm) transitions in Ne^+ (cf. Fig. 4) and the absolute cross sections for the energy-gain peaks A_{SC} and D_{SC} ($2.60\times10^{-16}+0.53\times10^{-16}$ cm^2 in Table I). Note that the sum of the cross sections for C_{SC}-E_{SC} in column 5 of Table I (from energy-gain data) is the same as the sum of the cross sections for the same process in column 6 (from C^{3+} photon-emission data). The (insignificant) differences between some of the individual cross sections are due to the rather uncertain relative intensity calibration for photons at 42.0 and 46.1 nm, which yields another relation between the cross sections for E_{SC} and $A_{SC}+D_{SC}$ than the energy-gain data [8].

Bloemen *et al.* [17] and Larsson *et al.* [10] have analyzed the corrections due to the relations between lifetimes and ion passage times (through the cell). Here we analyze the situation briefly for single-collision conditions (fulfilled here). The radiation emitted in the decay of populated projectile terms will then increase in intensity along the beam from the cell entrance until the rate of direct population and cascading to the term under study is equal to its decay rate. From this point the beam glows with constant intensity until it leaves the cell. This ''equilibrium'' in the fraction of carbon ions in a specific excited state occurs before the ions have reached the observation region if the term under study and important cascading terms are sufficiently short-lived. The upper terms of the present C^{2+} and C^{3+} transitions mostly have lifetimes below 10 ns, i.e., they are much shorter than the time of flight ($\sim$70 ns) from the cell entrance to the observation region [the exception is $C^{2+}(2s2p\ ^3P)$, which is metastable]. The emission intensities are thus nearly constant across the observation region, and σ_{em} for C^{2+} and C^{3+}

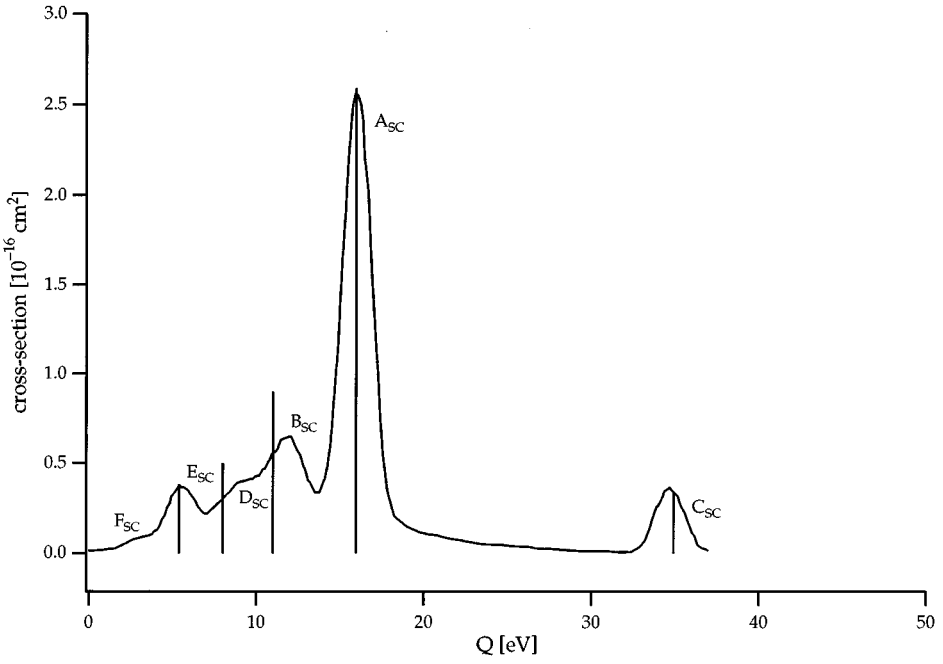

FIG. 3. Translational energy-gain spectrum for single-electron capture in 16 keV C^{4+}-Ne collisions from McCullough *et al.* ([7]). The labels A_{SC}–F_{SC} are explained in the text and in Table I. The absolute cross sections for specific collision processes with well-defined states for the target and the projectile after the collision are given as vertical lines (cf. text) and refers to the left-hand scale.

have been deduced directly from the calibration procedure (i.e., without lifetime corrections).

From the target, we observe a few Ne^+ and Ne^{2+} transitions and one transition from neutral Ne. The intensities of target spectral lines all increase linearly with increasing cell pressure, which shows that the target atoms emit the detected radiation before they collide with another Ne atom (such a secondary electron-capture collision would lead to emission at another wavelength). A comparison between typical target recoil energies (below 1 eV) and term lifetimes shows that the emission sequences are completed within a distance of 1 mm from the point of the excitation. A few Ne ions (atoms) created close to the edges may escape before they radiate, but this loss is compensated for by excited ions which are scattered into the observation region. One decay sequence is thus completed within the observation region for each target excitation event in the same region (except for the metastable excitations) and no correction factor was needed in order to determine σ_{em} for the target. We thus have a situation in which the emission cross sections for the target *and* the projectile can be determined directly from the calibration procedure described above. The largest absolute emission cross sections for spectra I and II are listed in Table II.

B. Term- and level-selective cross sections

From the emission cross sections and transition branching ratios in Table III, we deduce absolute cross sections for collision-induced population of specific atomic terms and levels (σ_{level}). These quantities are related to the probabilities for creations of specific excitations *directly in* the collisions (i.e., excluding cascading effects). All the spectral lines observed in this work have been identified and the atomic spectroscopy aspect of the data given in Table III is mostly

TABLE I. The assignments and Q values of the peaks A_{SC}–F_{SC} in the SC energy-gain spectrum for C^{4+}-Ne of McCullough *et al.* [8]. The absolute cross sections given in column 5 are obtained from a fit to this spectrum and normalization to the total cross section of Zwally and Koopmann [16], while those in columns 6 and 7, in addition, rely on the present photon-emission spectra (cf. text). The cross sections at 500 eV are from the energy-gain measurements of Cederquist *et al.* [3]. Only relative errors are given. There are additional errors due to the calibration procedure (12% for column 5 and 18% for columns 6 and 7). In columns 8 and 9, we give the wavelength of the emission from C^{3+} and Ne^+, respectively. The label g.s. denotes population of the ground state.

Peak	Collision products		σ (10^{-16} cm^2)				obs. emission (nm)	
label	$C^{4+}(1s^2\ ^1S) + Ne(2s^22p^6\ ^1S) \rightarrow$	Q (eV)	energy-gain 500 eV	energy-gain 16 keV	from C^{3+} emission	from Ne^+ emission	C^{3+}	Ne^+
A_{SC}	$C^{3+}(2s) + Ne^+(2s2p^6\ ^2S)$	16.0	1.1	} 2.60±0.01	-	} 2.59±0.34	g.s.	46.1
	$C^{3+}(2s) + Ne^+(2s^22p^43s\ ^2P)$	15.1	-		-		g.s.	44.6
B_{SC}	$C^{3+}(2s) + Ne^+(2s^22p^43s\ ^2D)$	12.4	-	} 0.90±0.07	-	<0.1	g.s.	40.6
	$C^{3+}(2s) + Ne^+(2s^22p^43p\ \ldots)$	8.9–11.8	-		-	-	g.s.	-
C_{SC}	$C^{3+}(2p) + Ne^+(2s^22p^5\ ^2P)$	34.9	-	0.36±0.01	0.33±0.13	-	155.0	g.s.
D_{SC}	$C^{3+}(2p) + Ne^+(2s2p^6\ ^2S)$	8.0	0.14	} 0.53±0.10	} 0.48±0.20	} 0.53±0.07	155.0	46.1
	$C^{3+}(2p) + Ne^+(2s2p^43s\ ^2P)$	7.1					155.0	44.6
E_{SC}	$C^{3+}(3s) + Ne^+(2s^22p^5\ ^2P)$	5.4	-	0.33±0.03	0.41±0.26	-	42.0	g.s.
F_{SC}		~3	--	0.09±0.02				

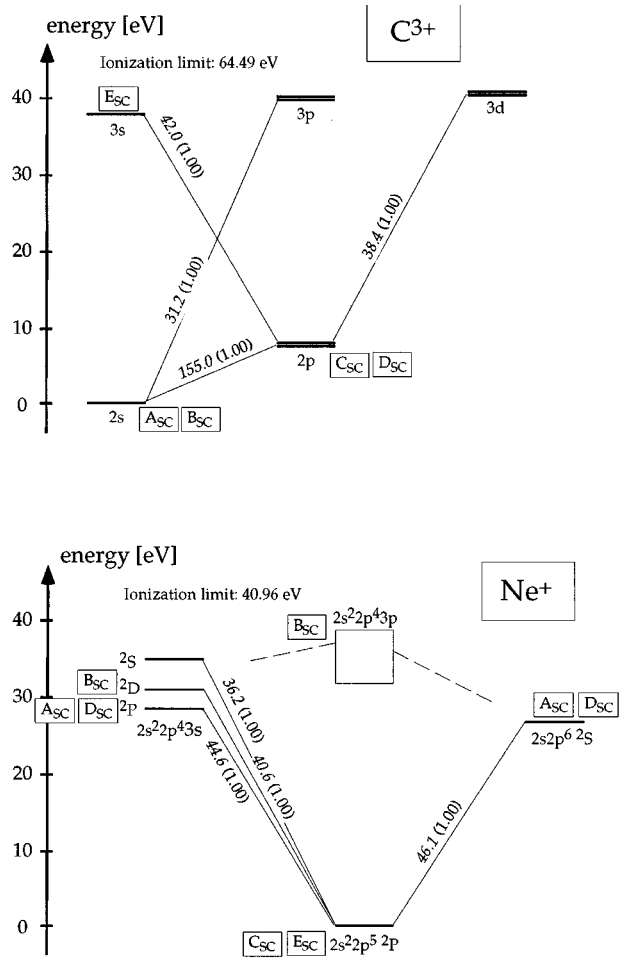

FIG. 4. Schematic energy-term diagrams for C^{3+} and Ne^{+}. Only transitions relevant for the present work are shown. Branching ratios are given within parentheses. The labels refer to various single-capture processes leading to population of specific energy terms in C^{3+} and Ne^{+}.

well known (cf. the database DAS and references given therein [18]). In the few cases where additional atomic data was needed, we used the HFR code by Cowan [15]. For Ne^{+}, we have neglected (the small) contributions from the few terms (only $2p^4 3p$) giving cascades with emission outside the scanned spectral regions (cf. Fig. 4).

C. Double-capture cross sections

Basically, we obtain σ_{DC}^{tot} in the following way: σ_{SC}^{tot} is first multiplied by the sum of term-selective cross sections for $C^{4+}+Ne \rightarrow C^{2+}+Ne^{2+}$ and then divided by the corresponding quantity for $C^{4+}+Ne \rightarrow C^{3+}+Ne^{+}$. This procedure would be fully correct if all the collision processes would lead to photon emission from the target *or* the projectile. This is indeed the case for a majority of the processes which we deal with here. However, we have to correct for the cases where no radiation was detected due to production of metastable and ground-state ions in the same collision (D_{DC} and E_{DC}) or emission outside the scanned spectral wavelength region (part of B_{SC}). We also have to compensate for cases with emission from projectile *and* target (D_{SC}; see Fig. 4). These corrections are all fairly small and they are easily performed with the aid of the relative intensity distributions in the energy-gain spectra for SC and DC (McCullough *et al.* [8]). We partition σ_{DC}^{tot} on the peaks (fitted to Gaussian curves) in the DC energy-gain spectrum in Fig. 5 [8] and the results from this procedure are presented in the fifth column of Table IV. The cross sections in columns six and seven of Table IV are determined directly from the absolute term-selective cross sections for C^{2+} and Ne^{2+} according to the procedures described in Secs. III A and III B.

TABLE II. Absolute emission cross sections, σ_{em}, and assignments of the most intense lines in the spectra due to 16 keV C^{4+}-Ne collisions. Some weaker lines of particular interest have been included. The line at 77.2 nm is due to a second-order reflection in the grating of the spectrometer. Since the corresponding first-order line falls outside the covered spectral region, we used the intensity of the second-order line to derive the emission cross section. Only relative errors are given here. There is an additional error of 18% in the absolute cross-section scale.

λ (nm)	Ion	Transitions	$\sigma_{em}(10^{-16}\ cm^2)$
	Spectrum I		
42.0	C^{3+}	2p–3s	0.41±0.26
44.6	Ne^{+}	$2s^22p^5\ ^2P–2s^22p^43s\ ^2P$	0.18±0.12
46.2	Ne^{+}	$2s^22p^5\ ^2P–2s2p^6\ ^2S$	2.94±0.39
49.0	Ne^{2+}	$2s^22p^4\ ^3P–2s2p^5\ ^3P$	1.37±0.17
53.8	C^{2+}	$2s2p\ ^3P–2s3s\ ^3S$	0.23±0.05
57.4	C^{2+}	$2s2p\ ^1P–2s3d\ ^1D$	0.14±0.03
69.0	C^{2+}	$2s2p\ ^1P–2s3s\ ^1S$	0.10±0.02
73.6	Ne	$2p^6\ ^1S_0–2p^53p\ ^1P_1$	0.08±0.03
77.2	C^{2+}(2nd)	$2s3s\ ^1S–2s3p\ ^1P$	<0.1
97.7	C^{2+}	$2s^2\ ^1S–2s2p\ ^1P$	13.4±1.9
	Spectrum II		
117.6	C^{2+}	$2s2p\ ^3P–2p^2\ ^3P$	0.48±0.06
124.7	C^{2+}	$2s2p\ ^1P–2p^2\ ^1S$	0.06±0.09
155.0	C^{3+}	2s–2p	1.22±0.20
229.7	C^{2+}	$2s2p\ ^1P–2p^2\ ^1D$	1.45±0.20

IV. RESOLVING TERM-SPECIFIC COLLISION PROCESSES

A. Single-electron capture

As mentioned above, McCullough *et al.* resolved six peaks (A_{SC}–F_{SC}) in the energy-gain spectrum for single-electron capture [8]. Two of the peaks (C_{SC} and E_{SC}) were assigned unambigously to a specific collision process and one was unidentified (F_{SC}) (cf. Table I). The remaining three could not be uniquely identified. In particular, it was not possible to discriminate between two possible (i.e., unresolved) processes for A_{SC} and D_{SC}. The two candidates for peak A_{SC} are processes populating the ground state of C^{3+}:

$$C^{4+}+Ne \rightarrow C^{3+}(2s\ ^2S)+Ne^{+}(2s2p^6\ ^2S) \qquad (1)$$

and

$$C^{4+}+Ne \rightarrow C^{3+}(2s\ ^2S)+Ne^{+}(2s^22p^43s\ ^2P) \qquad (2)$$

TABLE III. Absolute term- or level-selective cross sections, σ_{level}, for 16 keV C^{4+}-Ne collisions. The cross sections in the fourth column are σ_{em}, which are used together with corrections for the cascade situations to arrive at σ_{level}. The excitation energies above the ground state of the respective ions (atom) are given in column 2. Decay channels, wavelengths, and branching ratios (within parantheses) are given in the third column. Ground and metastable states are denoted by g.s. and m.s., respectively. Only relative errors are given in columns 4 and 5. There is an additional error of 18% in the absolute scale.

Level	Excitation energy (eV)	Decay channels λ (nm) and branching ratio	σ_{em} (10^{-16} cm^2)	σ_{level} (10^{-16} cm^2)
C^{3+}				
2s	0	g.s.		
2p	8.0	→2s: 155.0 (1.00)	1.22±0.20	0.81±0.33
3s	37.5	→2p: 42.0 (1.00)	0.41±0.26	0.41±0.26
3p	39.7	→2s: 31.2 (1.00)	-	-
3d	40.3	→2p: 38.4 (1.00)	<0.1	<0.1
C^{2+}				
$2s^2\ ^1S$	0	g.s.	-	-
$2s2p\ ^1P$	12.7	→$2s^2\ ^1S$: 97.7 (1.00)	13.4±1.9	11.6±1.9
$2p^2\ ^1D$	18.1	→$2s2p\ ^1P$: 229.7 (1.00)	1.45±0.20	1.45±0.20
$2p^2\ ^1S$	22.6	→$2s2p\ ^1P$: 124.7 (1.00)	0.06±0.09	0.06±0.09
$2s3s\ ^1S$	30.6	→$2s2p\ ^1P$: 69.0 (1.00)	0.10±0.02	0.10±0.02
$2s3p\ ^1P$	32.1	→$2s3s\ ^1S$: 38.6 (0.90)	<0.1	<0.1
		→$2p^2\ ^1D$: 88.4 (0.07)		
		→$2p^2\ ^1S$: 130.9 (0.02)		
$2s3d\ ^1D$	34.3	→$2s2p\ ^1P$: 57.4 (1.00)	0.14±0.03	0.14±0.03
$2s2p\ ^3P$	6.5	m.s.	-	-
$2p^2\ ^3P$	17.0	→$2s2p\ ^3P$: 117.6 (1.00)	0.48±0.06	0.48±0.06
$2s3s\ ^3S$	29.5	→$2s2p\ ^3P$: 53.8 (1.00)	0.23±0.05	0.23±0.05
$2s3p\ ^3P$	32.2	→$2s3s\ ^3S$: 465.1 (1.00)	0	0
$2s3d\ ^3D$	33.5	→$2s2p\ ^3P$: 46.0 (1.00)	0	0
Ne				
$2p^6\ ^1S_0$	0	g.s.	-	-
$2p^53s\ ^1P_1$	16.9	→$2p^6\ ^1S_0$: 73.6 (1.00)	0.08±0.03	0.08±0.03
$2p^53s\ ^3P_1$	16.7	→$2p^6\ ^1S_0$: 74.4 (1.00)	0	0
Ne^+				
$2s^22p^5\ ^2P$	0	g.s.	-	-
$2s2p^6\ ^2S$	26.9	→$2p^5\ ^2P$: 46.1 (1.00)	2.94±0.39	2.94±0.39
$2s^22p^43s\ ^2P$	27.8	→$2p^5\ ^2P$: 44.6 (1.00)	0.18±0.12	0.18±0.12
$2s^22p^43s\ ^2D$	30.6	→$2p^5\ ^2P$: 40.6 (1.00)	<0.1	<0.1
$2s^22p^43s\ ^2S$	34.3	→$2p^5\ ^2P$: 36.2 (1.00)	-	-
$2s^22p^43p$	31.2–37.9	→$2s2p^6$, $2p^43s$	-	-
Ne^{2+}				
$2s^22p^4\ ^3P$	0–0.1	g.s.	-	-
$2s2p^5\ ^3P$	25.4	→$2p^4\ ^3P$: 49.0 (1.00)	1.37±0.17	1.37±0.17
$2s^22p^4\ ^1D$	3.2	m.s.	-	-
$2s^22p^4\ ^1S$	6.9	m.s.	-	-
$2s2p^5\ ^1P$	35.9	→$2p^4\ ^1S_0$: 42.8 (0.10)	0	0
		→$2p^4\ ^1D_2$: 38.0 (0.90)	-	-

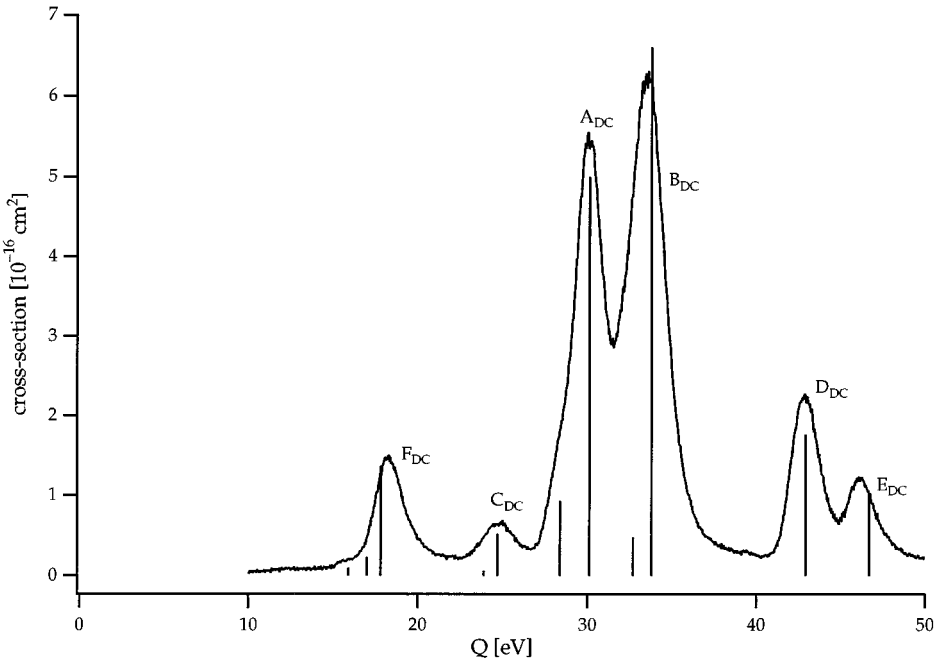

FIG. 5. Translational energy-gain spectrum for double-electron capture in 16 keV C^{4+}-Ne collisions from McCullough *et al.* ([7]). The labels A_{DC}–E_{DC} are explained in the text and in Table IV. The absolute cross sections for specific collision processes with well-defined states for the target and the projectile after the collision are given as vertical lines (cf. text) and refers to the left-hand scale.

at $Q=16.0$ eV and $Q=15.1$ eV, respectively. In this work, we are able to distinguish between these two final states of Ne^+ through a comparison between the term cross sections for $2s2p^6\ ^2S$ and $2p^43s\ ^2$P in Ne^+. The corresponding lines at 46.1 nm (the second strongest emission line in Table II) and 44.6 nm are to smaller extents due also to the D_{SC} processes

$$C^{4+}+Ne\rightarrow C^{3+}(2p\ ^2P)+Ne^+(2s2p^6\ ^2S) \qquad (3)$$

and

$$C^{4+}+Ne\rightarrow C^{3+}(2p\ ^2P)+Ne^+(2s^22p^43s\ ^2P) \qquad (4)$$

at $Q=8.0$ eV and $Q=7.1$ eV. Note that reactions (3) and (4) leave the Ne^+ target ion in the same excited states as reactions (1) and (2), respectively. Given the weakness of excitation to $2s^22p^43s$ compared to $2s2p^6$ excitation (cf. Table III), we conclude that reaction (1) dominates over reaction (2) and reaction (3) dominates over reaction (4). This conclusion is supported by the agreement in position between the Q value for reaction (1) and the A_{SC} peak of McCullough *et al.* [8], which is shown in Fig. 3. Note that a strong con-

TABLE IV. Absolute term-selective double-electron capture (DC) cross sections for specific resolved reaction channels in 16 keV C^{4+}-Ne collisions. The absolute cross sections in the sixth column are deduced according to Sec. IV C. Some of the unresolved processes in column 5 (deduced from the energy-gain spectrum of Fig. 5) are separated in columns 6 and 7 by means of the higher resolution of the present photon-spectroscopy data. Ground and metastable states are denoted by g.s. and m.s. in columns 8 and 9. Only relative errors are given. The errors in the absolute cross section scales are 21% (column 5) and 18 % (columns 6 and 7).

Peak	Collision products			σ (10^{-16} cm^2)			obs. emission (nm)	
label	$C^{4+}(1s^2\ ^1S)+Ne(2s^22p^6\ ^1S)\rightarrow$	Q (eV)	energy-gain 500 eV	energy-gain 16 keV	from C^{2+} emission	from Ne^{2+} emission	C^{2+}	Ne^{2+}
A_{DC}	$C^{2+}(2s2p\ ^1P)+Ne^{2+}(2s^22p^4\ ^1S)$	30.1	0.5±0.1	} 5.38±0.05	5.0±0.8	-	97.7	m.s.
	$C^{2+}(2p^2\ ^1D)+Ne^{2+}(2s^22p^4\ ^1D)$	28.4	0.8±0.1		0.93±0.13	-	229.7	m.s.
B_{DC}	$C^{2+}(2p^2\ ^3P)+Ne^{2+}(2s^22p^4\ ^3P)$	32.7	} 0.5±0.1	} 7.11±0.06	0.48±0.11	-	117.6	g.s.
	$C^{2+}(2s2p\ ^1P)+Ne^{2+}(2s^22p^4\ ^1D)$	33.8			6.6±1.1	-	97.7	m.s.
C_{DC}	$C^{2+}(2p^2\ ^1S)+Ne^{2+}(2s^22p^4\ ^1D)$	23.9	} <0.05	} 0.58±0.02	0.06±0.09	-	124.7	m.s.
	$C^{2+}(2p^2\ ^1D)+Ne^{2+}(2s^22p^4\ ^1S)$	24.7			0.52±0.07	-	229.7	m.s.
D_{DC}	$C^{2+}(2s^2\ ^1S)+Ne^{2+}(2s^22p^4\ ^1S)$	42.9	-	1.76±0.04	-	-	g.s.	m.s.
E_{DC}	$C^{2+}(2s^2\ ^1S)+Ne^{2+}(2s^22p^4\ ^1D)$	46.7	-	0.99±0.05	-	-	g.s.	m.s.
F_{DC}	$C^{2+}(2s2p\ ^3P)+Ne^{2+}(2s2p^5\ ^3P)$	17.8	-	1.37±0.04	-	1.37±0.22	m.s.	49.0
G_{DC}	$C^{2+}(2s3s\ ^1S)+Ne^{2+}(2s^22p^4\ ^1D)$	15.9	0.20±0.05	-	0.10±0.02	-	69.0	m.s.
H_{DC}	$C^{2+}(2s3s\ ^3S)+Ne^{2+}(2s^22p^4\ ^3P)$	17.0	-	-	0.23±0.05	-	53.8	m.s.
I_{DC}	$C^{2+}(2s3p\ ^1P)+\ldots$	?			<0.1		38.6	
	$C^{2+}(2s3d\ ^1D)+\ldots$	?			<0.1		57.4	

tribution from (2) would shift the latter peak towards lower values of Q. Thus, even though the channels (1) and (2) cross with the incident channel at very similar internuclear distances of $R \sim 5.1a_0$ and $R \sim 5.4a_0$, respectively, only the one with a suitable electronic configuration is populated efficiently. The behavior is the same for (3) and (4) with crossings at $10.2a_0$ and $11.5a_0$, respectively. This phenomenon simply reflects the fact that the one-electron rearrangements in reactions (1) and (3) (one electron is removed from the $2s$ shell of Ne) are strongly favored over the two-electron rearrangement in reactions (2) and (4) (one electron is removed from the $2p$ shell and another electron is simultaneously excited from $2p$ to $3s$). This effect was observed before at much lower energies ($\sim$500 eV) [3] and here we find that it is still very important at the much higher collision energy of 16 keV.

The energy-gain peak E_{SC} at $Q=5.4$ eV was ascribed to

$$C^{4+} + Ne \rightarrow C^{3+}(3s\ ^2S) + Ne^{+}(2s^2 2p^5\ ^2P) \qquad (5)$$

by McCullough *et al.* [8] and this is confirmed by the present detection of an emission line at 42.0 nm ($2p$-$3s$ in C^{3+}). The energy-gain peak B_{SC} in Table I was tentatively assigned to the processes

$$C^{4+} + Ne \rightarrow C^{3+}(2s\ ^2S) + Ne^{+}(2s^2 2p^4 3s\ ^2D) \qquad (6)$$

and

$$C^{4+} + Ne \rightarrow C^{3+}(2s\ ^2S) + Ne^{+}(2s^2 2p^4 3p \cdots), \qquad (7)$$

by McCullough *et al.* [8]. In the case of process (7), it was then stated that there might be contributions from LS terms of the $Ne^{+}(2p^4 3p)$ configuration with Q values ranging between 8.9 and 11.8 eV. The radiation from the decay of these Ne^{+} states fall outside the wavelength regime which is covered here. The emission at 40.6 nm from the excited Ne^{+} ion produced in reaction (6) is found to be very weak, indicating a cross section below 1×10^{-17} cm^2. Thus, from this reasoning it appears as if reaction (7) is dominant in B_{SC} and we have tentatively assigned the whole cross section (0.9×10^{-16} cm^2) to reaction (7) (average $Q=10.8$ eV). According to the energy-gain spectrum in Fig. 3 it also appears as if the contributions to reaction (7) with the highest Q values (11.8 eV) are dominant.

The summed cross section for capture to $C^{3+}(2s)$ is 3–4 times larger than the cross section for capture to $C^{3+}(2p)$. This difference is easily understood, since the crossing radii for population of $2p$ are either too small ($R=2.3a_0$ for C_{SC}) or too large ($R=10.2a_0$ for D_{SC}) in order for electron transfer to be very effective (i.e., the crossings lie outside the reaction window [3]). The reaction channels associated with $2s$ population, however, occur at more favorable internuclear separations, especially when they are associated with the removal of a $2s$ electron from Ne.

B. Double-electron capture

We determined the absolute double-electron capture cross section to $\sigma_{DC}^{tot}=(18\pm4)\times10^{-16}$ cm^2 (at 16 keV), which harmonizes with the result of Goldhar *et al.* of 23×10^{-16} cm^2 at 2 keV [19]. This is *a factor of 5* larger than the total cross section for single-electron capture, which is a very unusual situation in the field of multiply charged ion-atom collisions where the opposite relation often prevails. The larger of the term-selective cross sections in Table II are clearly related to collision processes which lead to population of electronic configurations in C^{2+} with the two outer electrons in $n=2$ states.

The cases were several collision processes contribute to population of the same term are treated in detail below, where we have separated the discussions of one- and two-step transfer mechanisms.

1. One-step transfer

Cederquist *et al.* [3] reported a cross section of 5×10^{-17} cm^2 for

$$C^{4+} + Ne \rightarrow C^{2+}(2p^2\ ^1D) + Ne^{2+}(2p^4\ ^1D) \qquad (8)$$

and a cross section of 8×10^{-17} cm^2 for

$$C^{4+} + Ne \rightarrow C^{2+}(2s2p\ ^1P) + Ne^{2+}(2p^4\ ^1S) \qquad (9)$$

at 500 eV collision energy. These processes were *not* resolved by McCullough *et al.* and they are denoted A_{DC} in Table IV [8]. The $2s2p\,^1P$ state in C^{2+} is created in collisions (9) and in one of the processes contributing to the (unresolved) energy-gain peak B_{DC} (cf. Fig. 5)

$$C^{4+} + Ne \rightarrow C^{2+}(2p^2\ ^3P) + Ne^{2+}(2p^4\ ^3P) \qquad (10)$$

and

$$C^{4+} + Ne \rightarrow C^{2+}(2s2p\ ^1P) + Ne^{2+}(2p^4\ ^1D). \qquad (11)$$

The $C^{2+}(2p^2\,^3P)$ state created in reaction (10) decays to $2s2p\ ^3P$ with emission at 117.6 nm. The dominating source of this radiation is most likely direct population via reaction (10) as can be seen in Fig. 6. [Other higher lying channels (H_{DC}, I_{DC}) leading to population of the C^{2+} triplet states are very weak (see Table IV) and significant cascades to $2p^2\ ^3P$ can be ruled out]. The cross section for reaction (10) can thus readily be determined to be 4.8×10^{-17} cm^2. Since we know the sum of the cross sections for reactions (10) and (11) (7.1×10^{-16} cm^2) from column five in Table IV, we are able to deduce also the absolute cross section for reaction (11) to be 6.6×10^{-16} cm^2. This is more than one order of magnitude larger than the cross section for (10) although the crossing radii with the incident channel are very similar, as can be seen in Fig. 7 [$R=3.3a_0$ for reaction (11) and $R=3.4a_0$ for reaction (10)]. Through a similar argument it is possible to deduce individual cross sections also for processes (8) and (9), with process (9) being the dominant one (5.0×10^{-16} cm^2) as can be seen in Table IV. In Fig. 7, we summarize the present results for single- (and double-) electron capture by showing the Q-value distribution together with the quasimolecular potential energy diagram.

The large magnitudes of the cross sections for $2s2p$ population at $Q=33.8$ and 30.1 eV of 6.6×10^{-16} cm^2 [process (11)] and 5.0×10^{-16} cm^2 [process (9)] strongly favors the picture of one-step transfer through the following argument: A hypothetical two-step mechanism would have to proceed via one of the SC channels with Q values 16 eV or

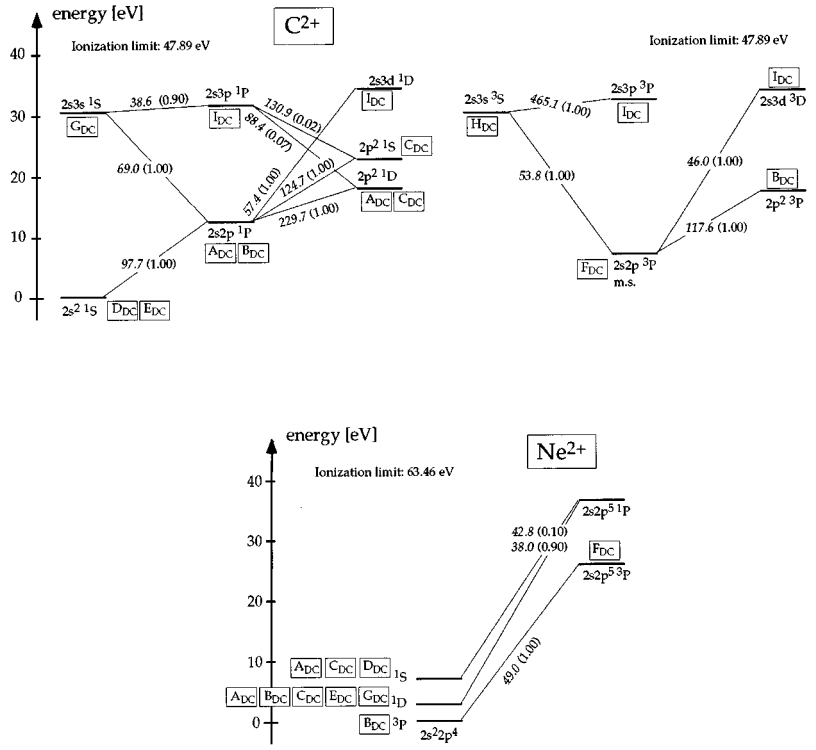

FIG. 6. Schematic energy-term diagrams for C^{2+} and Ne^{2+}. Only transitions relevant for the present work are shown. Branching ratios are given within parentheses. The labels refer to various double-capture processes leading to population of specific energy terms in C^{2+} and Ne^{2+}.

lower. The by far strongest of these channels, at $Q_{SC}=16.0$ eV, crosses with the $Q_{DC}=33.8$ eV channel at $\sim 1.5a_0$ (cf. Fig. 7) which would give a maximum (geometrical) cross section of $\sim 2\times 10^{-16}$ cm^2. This is significantly smaller than the measured cross sections for reactions (11) and (9) and thus this mechanism cannot be the dominant one. The outermost of the $2s2p$ channels crosses the incident channel at $3.6a_0$, giving a geometrical cross section of 11.5×10^{-16} cm^2, which is equal to the sum of the measured cross sections for the $Q=30.1$ and 33.8 eV channels. Since there are no other paths on the potential curves which could lead to processes (9) and (11) we regard it as very likely that the present $2s2p$ populations are due to one-step processes. This result is in line with the angular distributions measured by Keller *et al.* [9], who found evidence for a dominance of one-step two-electron transfer at much lower collision energy (~ 1 keV) for the four (then unresolved) DC channels around $Q=30$ eV. The present results for DC are shown together with the energy gain results of McCullough *et al.* in Fig. 5.

The Q values for channels (8)–(11) are 28.4, 30.1, 32.7, and 33.8 eV, respectively. Following the crossing points with

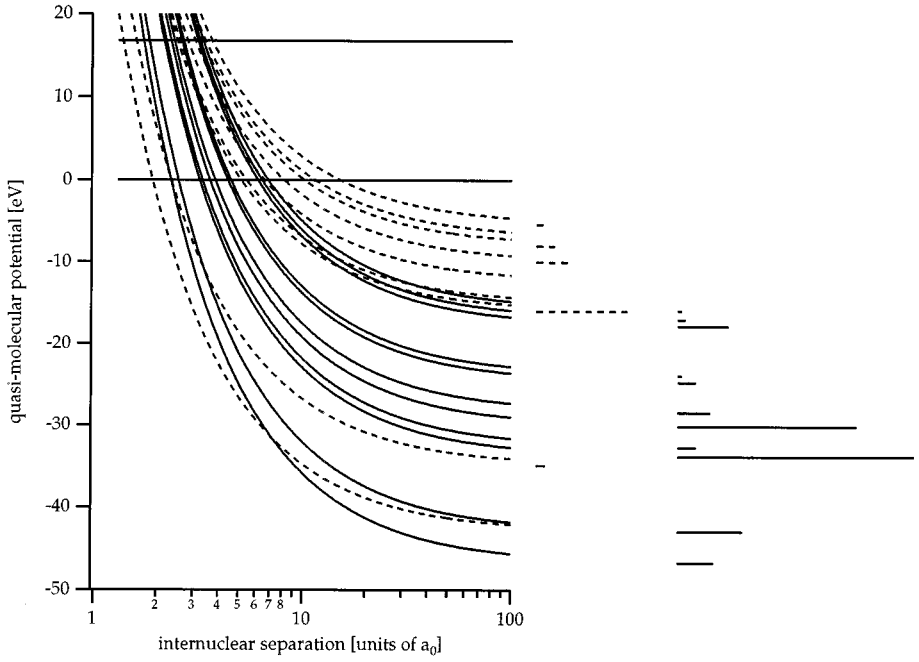

FIG. 7. High-resolution Q-value spectra for single- and double-electron capture in 16 keV C^{4+}-Ne collisions. Relative cross sections (linear scales; SC and DC cross sections can be compared directly) are shown as dashed and vertical bars to the right in the figure for SC and DC processes, repectively. The simplified diabatic quasimolecular potential curves (neglecting polarization and core penetration) are shown as dashed and full curves for SC and DC, respectively.

the incident channel for these four reaction channels (resolved in the present work) from larger to smaller values we find the following: A weak channel at $Q=28.4$ eV ($2p^2\ ^1D$ population in C^{2+}), followed by a strong channel at $Q=30.1$ eV ($2s2p\ ^1P$), then a weak channel at $Q=32.7$ eV ($2p^2\ ^3P$) and finally a strong channel at $Q=33.8$ eV ($2s2p\ ^1P$) (see Fig. 7). This ordering of the magnitudes of population cross sections as a function of crossing distance strongly indicates a substantial configuration selectivity—a preference for $2s2p$—for these *one-step* two-electron capture processes. Both $2s2p$ and $2p^2$ configurations can combine with their respective target states to form the same molecular symmetry, $^1\Sigma^+$, as the initial channel $C^{4+}(1s^2\ ^1S)$–$Ne(^1S)$. The LS terms for the projectile (^1D, ^1P, and ^3P) which are relevant in this context are all three strongly dominated (more than 99.9%) by their respective main configurations. It thus appears as if there is no artificial enhancement of electron transfer due to configuration interaction in the outgoing atomic states at infinite internuclear separation. Such effects could otherwise falsely indicate two-electron transfer at a single curve crossing if a nonnegligible configuration component leading to one-electron transitions would be present in either the initial or the final atomic states. This phenomenon was shown to be active in transfer excitation in Ar^{6+}-He collisions [20].

2. Two-step transfer

The metastable projectile state $2s2p\ ^3P$ in C^{2+} and the excited $2s2p^5\ ^3P$ Ne^{2+} state are populated in the process (F_{DC}; $Q_{DC}=17.8$ eV)

$$C^{4+}+Ne\rightarrow C^{2+}(2s2p\ ^3P)+Ne^{2+}(2s2p^5\ ^3P). \quad (12)$$

Emission from $Ne^{2+}(2s2p^5\ ^3P)$ is observed at 49.0 nm and we deduce a fairly large cross section of 1.4×10^{-16} cm^2 ($\sim$8% of σ_{DC}^{tot}) from the line intensity. At much lower collision energies (400–500 eV), Cederquist *et al.* found that another process (G_{DC}; $Q_{DC}=15.9$ eV),

$$C^{4+}+Ne\rightarrow C^{2+}(2s3s\ ^1S)+Ne^{2+}(2s^22p^4\ ^1D) \quad (13)$$

at $Q_{DC}=15.9$ eV, dominated the low-Q region completely [3]. In the present work at 16 keV we still find a small trace of process (13) through emission at 69.0 nm (cf. Figs. 1 and 6), but it is now more than ten times weaker than process (12). Keller *et al.* found a clear peak in the vicinity of $Q=16$ eV at their lowest energy (600 eV), while they found very little intensity in this region at 1 keV [9]. They [9] argued that process (13) probably was promoted by the closeness (in Q value) to the dominant SC process ($Q=16$ eV) at low collision energies ($\sim$0.5 keV). It was further speculated that this promotion perhaps was due to rotational coupling between the SC and DC channels close to $Q=16$ eV [(1) and (13)]. The strong shift in the relative population of processes (12) and (13) when going from 0.5 to 16 keV seems to further underscore the specialness of the population mechanisms for DC channels below $Q=20$ eV in C^{4+}-Ne collisions. The large crossing distances with the initial channel (see Fig. 7) for process (12) at $R=6.1\ a_0$ and process (13) at $R=6.8a_0$ make one-step transfer from the incident channel rather unlikely. This is shown by the results for the C^{4+}-He system, where two-electron capture to $2s^2$ at $R\sim2.3a_0$ dominates strongly over capture to $2s2p$ at $R\sim6.5a_0$ [21].

The reaction (12) at $Q=17.8$ eV leaves Ne^{2+} in an excited state ($2s2p^5\ ^3P$). The first step in a two-step process could then be a transition to the single-capture channel (3) at $R=10.2$ a.u. and $Q=8$ eV (leaving the target with a $2s$ hole) and the second step an inner crossing between processes (12) and (3) at $R=2.8a_0$. Such a scenario appears appealing since only one electron would have to change orbital at $R=10.2a_0$ and $R=2.8a_0$. The reaction channel (12) also crosses with the most important single-capture channel (1) at $R\sim14a_0$. This path on the potential curves is also, in principle, possible since the ''ionization potential'' of Ne^+ ($2s2p^6$) is sufficiently low in order to make electron transfer (of a $2p$ electron) to the projectile classically allowed (i.e., the internuclear potential barrier is sufficiently low [22]).

C. Excitation of Ne

In Table III, we have listed a small cross section ($\sigma_{ex}\sim8\times10^{-18}$ cm^2) for excitation of neutral Ne to the $2p^53s\ ^1P_1$ level, which is the lowest level which can be excited without violation of Wigner's spin-conservation rule (see, e.g., [3]). The collision velocity here is far too low for a direct excitation process to be feasible. Instead, it appears as if some curve crossing mechanism could be active since we are in the velocity region where electron capture is dominant. It is most likely that such a process would proceed as follows: First a transition from the incident quasimolecular channel to the dominant single-capture channel (1) at $Q_{SC}=16.0$ eV. In a second step there could be a transition from this channel to a channel leading to excitation without accompanying electron capture at an internuclear distance of $\sim3.5a_0$ (cf. Fig. 7)

$$C^{4+}+Ne\rightarrow C^{3+}(2s\ ^2S)+Ne^{+}(2s2p^6\ ^2S)$$
$$\rightarrow C^{4+}+Ne(2p^53s\ ^1P_1). \quad (14)$$

A two-step process leading to double-electron capture involving similar ranges of impact parameters would normally have a cross section in the 10^{-16} cm^2 range. The reason for the smallness of the cross section could be that the excitation process gives $Ne(2s^22p^53s\ ^1P_1)$, while the dominant SC process leaves the target in a $Ne^+(2s2p^6)$ configuration. It would thus be necessary with a two-electron rearranging process in the second step of process (14) at the $R=3.5a_0$ crossing.

V. CONCLUSION

We have shown, using photon-emission spectroscopy, that slow C^{4+}-Ne collisions exhibit many truly remarkable features. Both single- and double-electron capture are found to be *dominated by* processes in which the target is excited. These excitations are, however, mostly such that there are minimum changes in the electronic configurations of the projectile and the target. An inner $2s$ electron is removed from Ne in single-electron capture, while excited LS terms of the Ne^{2+} ground-state configuration often are produced in double-electron capture. The total cross section for double-

electron capture was found to be a factor of 5 larger than that for single-electron capture. In addition, the former process is found to be dominated by the one-step mechanism in which two electrons are transferred to the projectile at a single curve crossing. With the present photon-spectroscopy technique we have been able to separate several close-lying double-electron capture channels. This revealed a remarkable configuration selectivity in the population of $2s2p$ and $2p^2$ in C^{2+}, in which there was a strong preference for capture to $2s2p$, although the channels leading to $2p^2$ configurations cross with the incident channel at very similar internuclear separations.

We further report one marked difference between the population of double-electron capture channels at low ($\sim$ 0.5 keV [3]) and high (present 16 keV) energies. In the former study a reaction channel at $Q=15.9$ eV was dominant, but here we find a large contribution from a channel at $Q=17.8$ eV while the $Q=15.9$ eV channel is very weak.

We believe that the unusually strong role played by *one-step* two-electron transfer processes should make the C^{4+}-Ne collision system worthwhile to study in detail from a theoretical point of view. The present absolute cross sections for well-resolved reaction channels and the very weak configuration mixing in the final projectile states ought to make this an even more attractive prospect. Such calculations would perhaps also be able to shed some light on the mechanism behind the observed configuration selectivity for one-step two-electron capture.

ACKNOWLEDGEMENT

This work was supported by the Swedish Natural Science Research Council (NFR).

[1] M. Barat and P. Roncin, J. Phys. B **25**, 2205 (1992).
[2] D.H. Crandall, R.E. Olson, E.J. Shipsey, and J.C. Browne, Phys. Rev. Lett. **36**, 878 (1976).
[3] H. Cederquist, L.H. Andersen, P. Hvelplund, H. Knudsen, E.H. Nielsen, J.O.K. Pedersen and J. Sörensen, J. Phys. B **18**, 3951 (1985).
[4] N. Stolterfoht, C.C. Havener, R.A. Phaneuf, J.K. Swenson, S.M. Shafroth, and F.W. Meyer, Phys. Rev. Lett. **57**, 74 (1986).
[5] H. Winter, M. Mack, R. Hoekstra, A. Niehaus, and F.J. de Heer, Phys. Rev. Lett. **58**, 957 (1987).
[6] N. Stolterfoht, C.C. Havener, R.A. Phaneuf, J.K. Swenson, S.M. Shafroth, and F.W. Meyer, Phys. Rev. Lett. **58**, 958 (1987).
[7] H. Cederquist, C. Biedermann, N. Selberg, and P. Hvelplund, Phys. Rev. A **51**, 2169 (1995).
[8] R.W. McCullough, T.K. McLaughlin, T. Koizumi, and H.B. Gilbody, *1993 Proceedings of the 6th International Highly Charged Ion Conference (Kansas)*, AIP Conf. Proc. No. 274, edited by P. Richard, M. Stöckli, C.L. Cocke, and C.D. Lin (AIP, New York, 1994).
[9] N. Keller, R.D. Miller, M. Westerlind, S.B. Elston, I.A. Sellin, L.R. Andersson, C. Biedermann, and H. Cederquist, Phys. Rev. A **50**, 462 (1994).
[10] M.O. Larsson, A.M. Gonzalez, R. Hallin, F. Heijkenskjöld, R. Hutton, A. Langereis, B. Nyström, G. O'Sullivan, and A. Wännström, Phys. Scr. **51**, 69 (1995).
[11] M.O. Larsson, thesis Uppsala University, Uppsala, Sweden, 1995 (unpublished).
[12] M.O. Larsson, A.M. Gonzalez, R. Hallin, F. Heijkenskjöld, B. Nyström, G. O'Sullivan, C. Weber, and A. Wännström, Phys. Scr. **53**, 317 (1996).
[13] R. Hoekstra, F.J. de Heer, and R. Morgenstern, J. Phys. B **24**, 4025 (1991).
[14] M. Druetta and D. Hitz, Nucl. Instrum. Methods B **98**, 211 (1995).
[15] R.D. Cowan, *The Theory of Atomic Structure and Spectra* (University of California Press, Berkley 1986), and computer programs made available to us by Dr. Cowan.
[16] H.J. Zwally and D.W. Koopman, Phys. Rev. A **2**, 1851 (1970).
[17] E.W.P. Bloemen, D. Dijkamp D, and F.J. de Heer, J. Phys. B **15**, 1391 (1982).
[18] *DAS 1995 NIST Standard Reference Database 61, Database for Atomic Spectroscopy*, database development and integration by D.E. Kelleher, edited and compiled by W.C. Martin, J. Sugar, A. Musgrove, G.R. Dalton, W.L. Wiese, and J.R. Fuhr (NIST, Gaithersburg, MD, 1995).
[19] J. Goldhar, R. Mariella, Jr., and A. Javan, Appl. Phys. Lett. **29**, 96 (1976).
[20] L.R. Andersson, H. Cederquist, A. Bárány, L. Liljeby, C. Biedermann, J.C. Levin, N. Keller, S.B. Elston, J.P. Gibbons, K. Kimura, and I.A. Sellin, Phys. Rev. A **43**, 4075 (1991).
[21] M. Kimura and R.E. Olson, J. Phys. B **17**, L713 (1984).
[22] A. Bárány, G. Astner, H. Cederquist, H. Danared, S. Huldt, P. Hvelplund, A. Johnson, H. Knudsen, L. Liljeby, and K.-G. Rensfelt, Nucl. Instrum. Methods B **9**, 397 (1985).